Critical-point wedge filling and critical-point wetting

Alexandr Malijevský
Research Group of Molecular and Mesoscopic Modelling, The Czech Academy of Sciences, Institute of Chemical Process Fundamentals, 165 02 Prague, Czech Republic and Department of Physical Chemistry, University of Chemical Technology Prague, Prague 6, 166 28, Czech Republic

Andrew O. Parry
Department of Mathematics, Imperial College London, London SW7 2BZ, United Kingdom

(Received 27 November 2023; accepted 24 January 2024; published 14 February 2024)

For simple fluids adsorbed at a planar solid substrate (modeled as an inert wall) it is known that critical-point wetting, that is, the vanishing of the contact angle θ at a temperature T_w lying below that of the critical point T_c, need not occur. While critical-point wetting necessarily happens when the wall-fluid and fluid-fluid forces have the same range (e.g., both are long ranged or both short ranged) nonwetting gaps appear in the surface phase diagram when there is an imbalance between the ranges of these forces. Here we show that despite this, the convergence of the lines of constant contact angle, $0 < \theta < \pi$, to an ordinary surface phase transition at T_c, means that fluids adsorbed in wedges (and cones) always exhibit critical-point filling (wedge wetting or wedge drying) regardless of the range and imbalance of the forces. We illustrate the necessity of critical-point filling, even in the absence of critical-point wetting, using a microscopic model density functional theory of fluid adsorption in a right angle wedge, with dispersion and also retarded dispersionlike wall-fluid forces. The location and order of the filling phase boundaries are determined and shown to be in excellent agreement with exact thermodynamic requirements and also predictions for critical singularities based on interfacial models.

DOI: 10.1103/PhysRevE.109.024802

I. INTRODUCTION

Wetting transitions at solid-fluid interfaces and in fluid-fluid mixtures have been studied over the last five decades since first-order wetting transitions were first predicted by Cahn [1] and Ebner and Saam [2], for reviews see, for example, Refs. [3–7]. For wall-gas interfaces, as most directly pertinent to the present study, the wetting transition refers to the change from microscopic to macroscopic adsorption of liquid at a temperature T_w associated with the vanishing of the contact angle θ. Similarly, a drying transition refers to the divergence of the adsorption of gas at a wall-liquid interface, at temperature T_d, at which the contact angle becomes $\theta = \pi$. An interesting speculation of Cahn (based on what he thought were the temperature dependencies of the surface tensions) was that critical-point wetting and drying was necessary, that is, if partial wetting or partial drying occurs at low temperatures, a transition to complete wetting or complete drying must happen prior to the bulk critical temperature T_c. There have long been criticisms of the Cahn argument, particularly when long-ranged dispersion forces are present, suggesting that nonwetting may persist up to T_c in place of critical-point wetting [8]. Recent density functional theory (DFT) and simulation studies have clarified this determining the general structure of the surface phase diagrams for wetting in simple fluids when the fluid-fluid and wall-fluid forces are either short ranged (SR) or long ranged (LR) (i.e., decaying algebraically, as for dispersion forces) [9–11]. These build on the pioneering earlier study of Nakanishi and Fisher based on simpler Landau theory [12] and also later work by Ebner and Saam for Ising systems with a long-ranged surface field [13]. These studies show that, for wall-fluid interfaces, critical-point wetting or drying occurs, as per the speculation of Cahn, when the wall-fluid and fluid-fluid forces are similarly ranged but does not occur when one is LR and the other SR giving rise to nonwetting gaps in the phase diagram. However, the different possible surface phase diagrams all share key features, all stemming from the requirement that the terminus of the lines of temperature-driven wetting or drying transitions must correspond to a unique ordinary surface phase transition occurring at T_c [10]. This, superuniversal, structure of the surface phase diagrams has an interesting corollary for fluid adsorption in a wedge geometry (formed when two planar walls meet at a given opening angle) implying that it must be completely filled with liquid or with gas prior to the bulk critical point, i.e., while critical-point wetting may or may not occur for adsorption at a planar wall, fluids adsorbed in wedges always exhibit critical-point filling. The purpose of the present paper is to test this general prediction for a model DFT of wedge filling in a system with LR wall-fluid and SR fluid-fluid forces, which is known to exhibit a nonwetting gap, and to determine the global surface phase diagram showing the location and order of wedge wetting and wedge drying transitions.

II. WETTING AND WEDGE FILLING

A. Surface phase diagrams for wetting at wall-fluid interfaces

To begin we recall the different possible surface phase diagrams for wetting (of simple fluids) at a planar substrate and the subsequent implications for adsorption in wedge

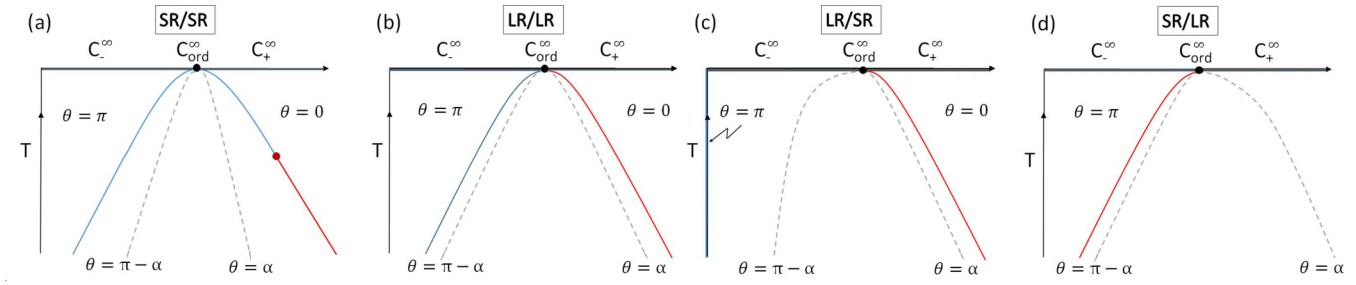

FIG. 1. Schematic illustration of four surface phase diagrams, in the (ϵ, T) plane, representing the different combinations of wall-fluid and fluid-fluid forces with long-ranged (LR) and short-ranged (SR) interactions. Continuous wetting and drying transitions are shown in blue, and in red if first order, as well as the regions of complete wetting and drying. Lines of temperature-driven wetting and drying always terminate at an ordinary surface phase transition, $C^{\infty}_{\rm ord}$, separating lines of critical desorption, C^{∞}_{-}, and critical adsorption, C^{∞}_{+}, at the critical temperature T_c. All lines of constant contact angle, $0 < \pi < \theta$, converge to $C^{\infty}_{\rm ord}$. Only the line of continuous drying occurring exactly at $\epsilon = 0$ for the LR-SR system does not converge to $C^{\infty}_{\rm ord}$. SR-SR and LR-LR systems exhibit critical-point wetting while LR-SR and SR-LR systems show nonwetting gaps, in which the contact angle tends to 0 (SR-LR) and π (LR-SR) as $T \to T_c$.

geometries. Consider the interface between a solid substrate, modeled as an inert planar wall, situated in the $z = 0$ plane and a bulk fluid at temperature T and chemical potential μ. The fluid particles interact via a pair potential, for which we denote the attractive part $\phi_{\rm att}(r)$, and suppose this gives rise to bulk coexistence between gas (g) and liquid (l) phases along a saturation curve $\mu_{\rm sat}(T)$ up to a critical point at temperature T_c. For systems with SR forces the potential $\phi_{\rm att}(r)$ is truncated at a finite range, while it decays as $\phi_{\rm att}(r) \propto -r^{-6}$ for dispersion forces and $\phi_{\rm att}(r) \propto -r^{-7}$ for retarded dispersion forces. The wall also exerts an external potential $V(z)$ on the fluid particles, which contains an attractive part of strength ϵ and a hard-wall contribution $V(z) = \infty$ for $z < 0$. For systems with SR forces we may imagine that $V(z)$ has strictly finite range or is exponentially decaying, while with LR forces it decays as $V(z) = -\epsilon z^{-p}$ with $p = 3$ for dispersion forces and $p = 4$ for retarded dispersion forces. The wall-gas ($\mu = \mu^{-}_{\rm sat}$) and wall-liquid ($\mu = \mu^{+}_{\rm sat}$) interfaces have distinct equilibrium density profiles $\rho(z)$ and distinct surface tensions $\gamma_{\rm wg}$ and $\gamma_{\rm wl}$, which can be determined using, for example, microscopic DFT models. From these we can then identify the equilibrium contact angle from Young's equation [14]

$$\gamma_{\rm wg} = \gamma_{\rm wl} + \gamma_{\rm lg}\cos\theta, \tag{1}$$

where $\gamma_{\rm lg}$ is the liquid-gas tension. The surface phase diagram, plotted in the (ϵ, T) plane, then shows lines of wetting transitions and drying transitions where the contact angle vanishes and approaches π, respectively. Depending on the range and balance of the wall-fluid and fluid-fluid forces the different possible phase diagrams can, at first sight, appear markedly different, with some exhibiting critical-point wetting while others showing nonwetting all the way to T_c [9]. However, these dissimilarities become less mysterious when we add the loci of lines of constant contact angle, $0 < \theta < \pi$ and also mark the location of the ordinary surface phase transition, $C^{\infty}_{\rm ord}$, separating the lines of critical desorption C^{∞}_{-} and critical adsorption C^{∞}_{+}, occurring at T_c [11]. Schematic portraits of four surface phase diagrams, obtained from DFT and simulation studies, representing the different combinations, SR-SR, LR-LR, LR-SR, and SR-LR for the ranges of the wall-fluid and fluid-fluid forces are shown in Fig. 1. In these diagrams, the continuous blue lines represent the lines of continuous wetting and drying transitions where the adsorption diverges continuously on approaching from the region of partial wetting or drying. Red lines denote first-order wetting and drying phase boundaries, where the adsorption jumps from a microscopic to macroscopic value. The phase diagrams for SR-SR and LR-LR systems are similar with each exhibiting critical-point wetting and drying since the lines of both wetting and drying transitions converge to an ordinary surface phase transition $C^{\infty}_{\rm ord}$. The phase diagrams for these systems, with balanced ranges of the wall-fluid and fluid-fluid forces, are similar to that predicted by Nakanishi and Fisher using Landau theory and general scaling arguments although the location of tricritical wetting points is model specific. However, when the forces are imbalanced, as for LR-SR and SR-LR systems, the surface phase diagrams exhibit nonwetting gaps [9]. For LR-SR systems only the line of first-order wetting ends at $C^{\infty}_{\rm ord}$, while the line of temperature-independent continuous drying transitions, located exactly at $\epsilon = 0$, ends at a point along the line of critical desorption. There is therefore a nonwetting gap in the surface phase diagram between $\epsilon = 0$, corresponding to a pure hard wall, and $\epsilon = \epsilon^c$, corresponding to the location of the ordinary surface phase transition, a feature, which was anticipated by de Gennes who was the first to point out the consequences for wetting when LR wall-fluid forces are present [15] (see also Privman [16]). Within the nonwetting gap the contact angle $\theta \to \pi$ as $t \equiv (T_c - T)/T_c \to 0$ with a power law depending on the range of the forces. For systems with dispersion forces mean-field (MF) theories predict $\pi - \theta \propto -1/\ln t$ (corresponding to marginal behavior) while more correctly it is estimated that $\pi - \theta \propto t^{\psi_{\rm LS}}$ with $\psi_{\rm LS} \approx 0.16$ allowing for the nonclassical values of bulk critical exponents [11]. For SR-LR systems on the other hand the surface phase diagram shows only a line of first-order drying transitions, which terminates at an ordinary surface phase transition $C^{\infty}_{\rm ord}$, and hence has an infinite nonwetting gap for $\epsilon > \epsilon^c$. Within this gap the contact angle vanishes as $T \to T_c$, following the power law $\theta \propto t^{\psi_{\rm SL}}$ where $\psi_{\rm SL} \approx 0.77$ for systems with dispersion forces (with $\psi_{\rm SL} = 1/2$ at MF level) [11].

Despite the presence of nonwetting for LR-SR and SR-LR systems, in contrast with critical-point wetting for SR-SR and LR-LR systems, there are key features, which are common

to all the phase diagrams. At T_c all the surface phase diagrams have a unique ordinary surface phase transition, $C^{\infty}_{\rm ord}$, occurring at $\epsilon = \epsilon^c$ (the value of which is system specific). Either side of this are lines of critical desorption, C^{∞}_{-}, and critical adsorption, $C^{\infty}_{\rm ord}$, along which the profile decays to the bulk critical density as $\rho(z) - \rho_c \approx \pm z^{-\beta/\nu}$. Here β and ν are the standard bulk critical exponents for the difference in the bulk liquid and gas densities, $\Delta\rho \propto t^{\beta}$ and the bulk correlation lengths $\xi_g, \xi_l \propto t^{-\nu}$. For completion we note that exactly at $C^{\infty}_{\rm ord}$ the density profile has a faster decay towards ρ_c, the exponent for which depends on the range of the forces but will not be needed here [10]. In all four phase diagrams the limiting value of the contact angle is $\theta = \pi$ for $\epsilon < \epsilon^c$ and $\theta = 0$ for $\epsilon > \epsilon^c$. A crucial common feature, stemming from this, is that the lines of constant contact angle, $0 < \theta < \pi$ (as well as temperature-driven wetting and drying phase boundaries), converge to $C^{\infty}_{\rm ord}$ regardless of the presence of critical-point wetting or of nonwetting. These are shown as the dashed lines in Fig. 1, which correspond to the lines of constant contact angle $\theta = \alpha$ and $\theta = \pi - \alpha$, where we may choose any value $0 < \alpha < \pi/2$. This superuniversal property of the lines of constant contact angle is consistent with the scaling theory of Nakanishi and Fisher, which implies that they follow trajectories $t_\theta \propto c(\theta)|\epsilon^c - \epsilon|^{1/\Delta_1}$ where Δ_1 is the surface gap exponent for the ordinary surface phase transition (which takes the value $\Delta_1 = 1/2$ at MF level) [12]. The constant of proportionality $c(\theta)$ is not determined by scaling theory, but for systems with an Ising symmetry must obey $c(\pi/2) = 0$. We anticipate similar behavior occurs for SR-SR and LR-LR systems. Critical-point wetting or drying occurs provided $c(0)$ and $c(\pi)$ are nonzero. The appearance of a nonwetting gap for the LR-SR system can then be seen as a limit in which the line of drying transitions is deformed to $\epsilon = 0$ (and is hence temperature independent) with the constant of proportionality vanishing as $c(\theta) \propto (\pi - \theta)^{1/\psi_{\rm LS}}$ so that $c(\pi) = 0$, i.e., there is no critical-point drying and $\theta \to \pi$ only in the limit $T \to T_c$. Similarly, the nonwetting gap for SR-LR systems corresponds to the line of wetting transitions being deformed to $\epsilon = \infty$, and the constant of proportionality vanishes as $c(\theta) \propto \theta^{1/\psi_{\rm SL}}$, so that in this case $c(0) = 0$ implying that $\theta \to 0$ only as $T \to T_c$. We mention that the present discussion of nonwetting, arising from the imbalance of the wall-fluid and fluid-fluid forces, is focused on solid (wall)-fluid interfaces. By a wall, we mean specifically that the external potential $V(z)$ contains both an attractive part, of strength ϵ, acting on fluid particles in the half-space $z > 0$ and an impenetrable hard-wall contribution for $z < 0$. For these systems the topology of the surface phase diagram is constrained by the existence of the ordinary surface phase transition $C^{\infty}_{\rm ord}$. Wetting transitions and nonwetting also occur in other systems, for example, in fluid-fluid mixtures and grain boundaries where the analog of a surface field strength ϵ and the impenetrable hard-wall constraint is missing. The phase diagrams for these systems are no longer constrained by the presence of a unique ordinary surface phase transition at a given value of ϵ_c and the conditions for nonwetting are different. For example, simple models of interfaces in ternary mixtures with purely SR forces show that nonwetting occurs along a large segment of the line of critical end points along which the relevant dihedral contact angle does not vanish [17]. While not of relevance to our discussion of wedge filling, this indicates that there are likely different types of nonwetting pertinent to wall-fluid and fluid-fluid systems.

B. Binding potentials

A very useful, and much used, way of modeling wetting transitions is via the use of a binding potential $W(\ell)$, corresponding to the free energy of a wetting layer of constrained, uniform, thickness ℓ [3–7]. This is usually constructed from an underlying microscopic description, for example a Landau-Ginzburg-Wilson model for SR-SR systems or a DFT model $\Omega[\rho]$ where the constraint on the film thickness is applied using a mean-field-like approximation. For continuous wetting transitions the binding potential is repulsive at short distances, attractive at larger distances possessing a single minimum, which determines the equilibrium MF thickness of the wetting layer, which diverges continuously approaching T_w. The curvature of $W(\ell)$ at this point then determines the parallel correlation length from $\xi_\parallel = \sqrt{\gamma_{\rm lg}/W''}$, which also diverges continuously. For first-order wetting transitions on the other hand, a potential barrier separates the minimum in $W(\ell)$ (close to the wall) and at $\ell = \infty$ (corresponding to the completely wet state), which coexist at T_w. Fluctuation effects, beyond MF, are then incorporated using an approximate effective interfacial Hamiltonian, which in its simplest form is given by

$$H[\ell] = \int d\mathbf{x}\left[\frac{\gamma_{\rm lg}}{2}(\boldsymbol{\nabla}\ell)^2 + W(\ell)\right] \tag{2}$$

and includes the energy cost incurred by thermal fluctuations, which increase the interfacial area of the unbinding liquid-gas interface. While the use of binding potentials and interfacial Hamiltonians at wetting transitions is very well established, their application to each of the four surface phase diagrams shown in Fig. 1 comes with some caveats, which we discuss here.

For each of the wetting phase diagrams we should distinguish between the binding potential constructed for the wetting (w) and drying (d) transitions, pertinent to the wall-gas and wall-liquid interfaces respectively. For SR-SR systems, the binding potential $W^{(w)}_{\rm SS}(\ell)$ describing the wetting transition is usually written as a sum of exponentials [18–20]

$$W^{(w)}_{\rm SS}(\ell) = ae^{-\kappa_l \ell} + be^{-2\kappa_l \ell} + \cdots, \tag{3}$$

where $\kappa_l = 1/\xi_l$ is the inverse of the true correlation length of the bulk liquid and we have assumed here, and below, that we are at bulk coexistence, $\mu = \mu^{-}_{\rm sat}$. A similar expression describes the binding potential for drying, $W^{(d)}_{\rm SS}$, constructed for the wall-liquid interface, but the exponential decay is controlled by the inverse bulk gas correlation length $\kappa_g = 1/\xi_g$. The coefficients a and b are determined by the fields ϵ and T leading to the phase boundaries appearing in surface phase diagram Fig. 1(a). The MF continuous wetting (drying) phase boundaries then correspond to the condition $a = 0$, provided $b > 0$, with the transition being first-order if $b < 0$. Even at MF level, however, this description assumes that subdominant oscillatory decaying contributions to $W_{\rm SS}(\ell)$ are unimportant, i.e., T_w is sufficiently far above the temperature $T_{\rm FW}$ of the intersection of the Fisher-Widom with the bulk coexistence

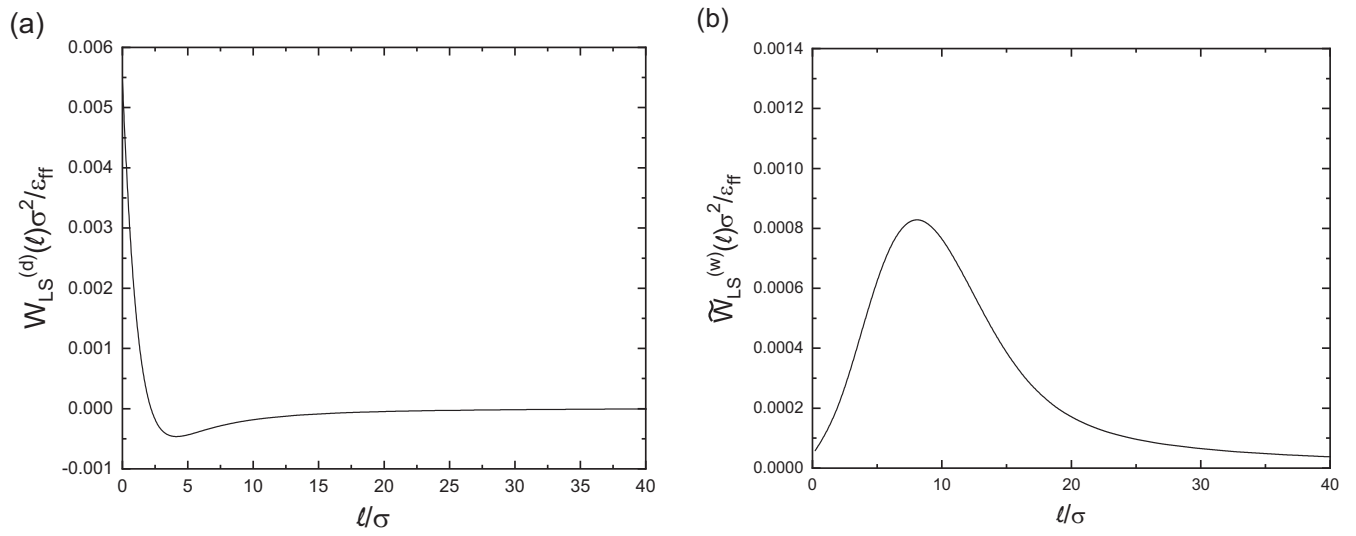

FIG. 2. Numerically determined binding potentials for (a) continuous drying and (b) first-order wetting transitions in LR-SR systems with dispersionlike wall-fluid forces, $V(z) = -\epsilon_3/z^3$, obtained from a microscopic DFT. In the vicinity of the drying transition, pertinent to the wall-liquid interface at $\epsilon_3 = 0$, the binding potential $W_{\rm LS}^{(d)}(\ell)$, has a well-defined minimum, determining the equilibrium MF drying layer thickness, shown for $\epsilon_3 = 0.2$ and $T/T_c = 0.92$. For the wetting transition, pertinent to the wall-gas interface, only a partial binding potential, $\tilde{W}_{\rm LS}(\ell)^{(w)}$, describing the tail of the binding potential, may be determined. This does not possess a local minimum near the wall since, even at the wetting temperature $T_w = 0.93\,T_c$, shown for $\epsilon_3 = 2$, no wetting layer of liquid has formed at the wall-gas interface. Units here are σ, the hard-sphere diameter, and $\epsilon_{\rm ff}$, the strength of the fluid-fluid potential.

curve that $2\kappa_l < \kappa_{\rm osc}$ where $\kappa_{\rm osc}$ is the inverse length scale determining the leading oscillatory decaying terms [21]. A similar caveat applies even for the drying transition despite the absence of a Fisher-Widom line in the bulk gas region of the phase diagram. Moreover, to properly model fluctuation effects beyond MF at continuous, tricritical, and first-order wetting transitions, one must also include an entropic Casimir contribution to the binding potential, missing in MF descriptions, coming from microscopic fluctuations that correspond to the same interfacial position and also allow for nonlocal effects to avoid nonphysical instabilities [22–24].

For LR-LR systems, say with dispersion forces, the binding potential for wetting (and drying) is determined as [25]

$$W_{\rm LL}^{(w)}(\ell) = \frac{a_2}{\ell^2} + \frac{a_3}{\ell^3} + \cdots, \tag{4}$$

where, again, the condition $a_2 = 0$ determines the continuous wetting phase boundary in the phase diagram, provided that $a_3 > 0$. The value of a_2 can be determined using a simple sharp-kink approximation in which the wetting or drying layer is modeled as a structureless slab of liquid or gas. In order to understand the correct structure of the phase diagram Fig. 1(b), including, the order of the lines of wetting and drying transitions, and their required convergence to $C_{\rm ord}^{\infty}$, soft-kink contributions to higher coefficients a_3, a_4, arising from the local adsorption of fluid at the wall, must be included and also a resonant term $\ln \ell/\ell^5$ arising from the overlap of the potential $V(z) \propto 1/z^3$ with the algebraic decay in the density profile from the liquid-gas interface induced by the fluid-fluid dispersion forces [10]. For the systems exhibiting nonwetting gaps, even more stringent caveats apply. For the above two cases of SR-SR and LR-LR systems discussed above, both the wetting and drying transitions can each be modeled and understood using a binding potential within an effective Hamiltonian description. However, this is no longer the case when there is an imbalance between the wall-fluid and fluid-fluid forces since the wetting and drying transitions may have very different characters. Let us consider LR-SR systems first. The continuous drying transition occurring at $\epsilon_p = 0$ for the wall-liquid interface can be understood using a binding potential, which takes the form [9]

$$W_{\rm LS}^{(d)}(\ell) = -\frac{\Delta\rho\epsilon_p}{(p-1)\ell^{p-1}} + ae^{-\kappa_g\ell} + \cdots, \tag{5}$$

incorporating a long-ranged attraction from the tail of the wall-fluid potential, $V(z) = -\epsilon_p z^{-p}$, and a short-ranged repulsion arising from the hard wall (with $a > 0$). This binding potential possesses a minimum, determining the equilibrium (MF) thickness of the drying layer, the location of which diverges as $\epsilon \to 0$. In Fig. 2(a), we show a plot of the binding potential $W_{\rm LS}^{(d)}(\ell)$ determined numerically from an underlying microscopic DFT (described in the next section) corresponding to partial minimization of the grand potential functional $\Omega[\rho]$ (per unit area) under the constraint that the drying layer of gas is of thickness ℓ [where $\rho = (\rho_g + \rho_l)/2$]. However, no such binding potential can be constructed for the wetting transition since the transition is so strongly first order that even at the wetting temperature T_w no thick wetting layer of liquid has yet formed at the wall-gas interface. This is illustrated in Fig. 3, where we plot the equilibrium density profile $\rho(z)$ for the wall-gas interface at $T = T_w = 0.92\,T_c$ obtained using a microscopic DFT; clearly no liquid wetting layer has yet been formed although some minor local layering is present. In this case we can only construct a partial binding potential $\tilde{W}_{\rm LS}^{(w)}(\ell)$ describing the excess free-energy cost of a thick wetting layer, but which never corresponds to the actual, partially wet, equilibrium density profile. We can anticipate that this partial binding potential contains an algebraic repulsion

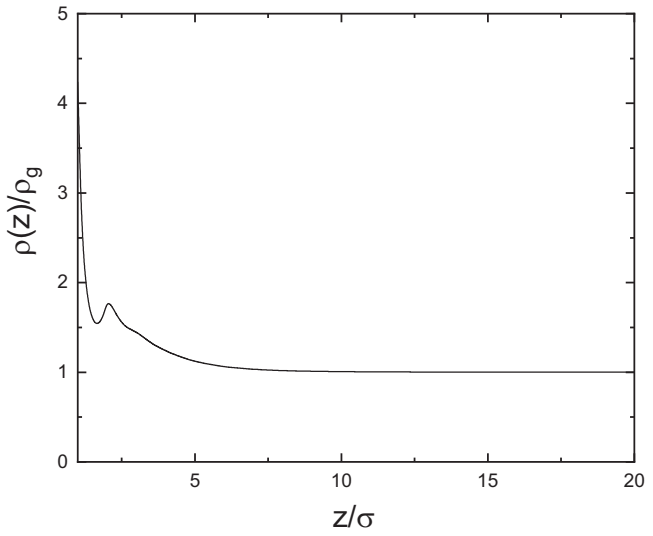

FIG. 3. DFT results for the equilibrium density profile $\rho(z)$, for the wall-gas interface, at a first-order wetting transition for LR-SR systems with dispersionlike wall-fluid forces showing that no wetting layer of liquid has formed at the wall. This phase coexists with one in which there is a macroscopic layer of liquid adsorbed at the wall, there is only some minor layering associated with local packing effects. Here $\epsilon_3 = 2$ and $T_w = 0.92\,T_c$.

$\tilde{W}_{\rm LS}^{(w)}(\ell) \sim \Delta\rho\epsilon_p/(p-1)\ell^{p-1}$ coming from the tail of the wall-fluid potential and also an activation barrier coming from a short-ranged attraction. This is illustrated in Fig. 2(b) where we show the partial binding potential constructed numerically from a DFT model via constrained minimization of the grand potential functional under the constraint that the profile satisfies $\rho(\ell) = (\rho_g + \rho_l)/2$. Such strongly first-order wetting transitions cannot be described using a two-dimensional (2D) effective Hamiltonian (2), and instead require a full 3D description, afforded by a fully microscopic DFT. This also happens in Landau theory descriptions of SR wetting transitions in simple magnets, with negative surface enhancement, where the wetting transition is again so strongly first order that no wetting layer has formed. In this case an abrupt dimensional reduction from 3D- to 2D-like behavior occurs, via a nonthermodynamic singularity [26]. It is only in the 2D regime, where the parallel correlation length $\xi_\parallel > \xi_l$ that an effective Hamiltonian description is possible. For the present LR-SR systems we suspect that the whole line of first-order wetting transitions belongs to the 3D regime, where the properties of the wall-gas interface can only be modeled using a fully microscopic description.

C. Surface phase diagrams for wedge filling

The common properties of the lines of constant contact angle, $0 < \theta < \pi$, across all four systems, has immediate repercussions for the location of filling (wedge wetting or wedge drying) phase boundaries for fluids adsorbed in wedge geometries. Consider a wedge formed by two identical planar walls that meet at an opening angle $\pi - 2\alpha$, so that the planes of the wall lie at tilt angles $\pm\alpha$ to the horizontal plane $z = 0$ (say). Translation invariance is assumed in the third dimension along the wedge. As above we suppose that the wedge is contact with a bulk fluid at chemical potential μ and (subcritical) temperature T_c. The wedge may be thought of a missing link between a planar wall geometry ($\alpha = 0$) and a narrow capillary slit ($\alpha = \pi/2$) and itself shows a surface phase transition distinct from the wetting and capillary condensation pertinent to these limits. Far from the wedge apex, the adsorption of the fluid near the walls will be same as that for planar geometry. However, near the apex, the confining geometry enhances the local adsorption of liquid at a wedge-gas interface, and the enhances the local adsorption of gas at a wedge-liquid interface. In fact macroscopic arguments dictate that a wedge-gas interface, at $\mu = \mu_{\rm sat}^-$, is completely filled by liquid above a wedge wetting temperature T_{ww}, which occurs when the contact angle $\theta(T)$ corresponding to the planar wall, satisfies [28,29]

$$\theta(T_{ww}) = \alpha. \tag{6}$$

Similarly, a wedge-liquid interface, at $\mu = \mu_{\rm sat}^+$, is completely filled by gas above a wedge drying temperature $T_{\rm wd}$, when the contact angle satisfies

$$\theta(T_{\rm wd}) = \pi - \alpha. \tag{7}$$

Wedge wetting and wedge drying transitions correspond to the formation of a macroscopic meniscus at the wedge apex. The transition may be continuous or first-order corresponding to the continuous or discontinuous divergence of the height, ℓ_w, of the liquid-gas interface, measured above the wedge apex, at the filling phase boundary.

Wedge filling transitions are associated with the formation of a macroscopic meniscus and the vanishing of a wedge contact angle, θ_w, satisfying Wenzel's law,

$$\cos\theta_w = \cos\theta\,\sec\alpha, \tag{8}$$

which specifies the exact angle with which a macroscopic drop must meet the apex line (as opposed to the side walls). Intriguingly, this phenomenon was observed experimentally, in beautiful drop tower studies several years before the first work on wetting transitions, see the monograph [27]. Filling transitions may be first order or continuous corresponding to the discontinuous or continuous change from microscopic to macroscopic adsorption near the apex. For continuous filling transitions we may define exponents for the divergence of the local film thickness (the height of the liquid-gas interface above the apex), ℓ_w, (see Fig. 2) the local interfacial roughness, $\xi_\perp$, and the correlation length ξ_y associated with interfacial fluctuations along the wedge:

$$\ell_w \propto (\theta-\alpha)^{-\beta_w}, \qquad \xi_\perp \propto (\theta-\alpha)^{-\nu_\perp}, \qquad \xi_y \propto (\theta-\alpha)^{-\nu_y}. \tag{9}$$

The values of these exponents are, in general, distinct from those characterizing continuous wetting transitions, except in two dimensions, where filling and wetting are related precisely by the local symmetry of wedge covariance [30–32].

Before discussing the values of the exponents, it is apparent immediately that the universal convergence of the lines of constant contact angle to $C_{\rm ord}^\infty$ implies that critical-point filling occurs in all systems. Indeed, the lines of constant contact angle $\theta = \alpha$ and $\pi - \theta = \alpha$ in the wetting phase diagrams

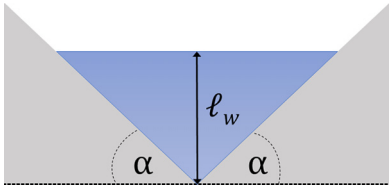

FIG. 4. Schematic illustration of the adsorption of a liquid layer, of thickness ℓ_w, near the apex of a wedge with opening angle $\pi - 2\alpha$ in contact with bulk gas at saturation chemical potential. The wedge is completely filled with liquid if the contact angle $\theta < \alpha$. Similarly a wedge-liquid interface is completely filled with gas if $\pi - \theta < \alpha$.

also determine the exact filling phase boundaries for wedge wetting and wedge drying. It follows that critical-point filling occurs in the presence of critical-point wetting (SR-SR and LR-LR) or of nonwetting (LR-SR and SR-LR). The corresponding surface phase diagrams for filling (wedge wetting and wedge drying) are shown schematically in Fig. 4 where we have again used blue and red to denote the location of the lines of continuous and first-order filling, respectively. In all these diagrams the lines of wedge wetting and wedge drying converge to the same location of the corresponding ordinary surface phase transition. Studies based on effective Hamiltonians for filling transitions in shallow wedges (small α) indicate that the order of the filling transition can be inferred from the order of the wetting transitions pertinent to the side walls and the structure of the binding potential $W(\ell)$. For example at MF level the height of the filling layer is determined as [33]

$$\gamma_{\rm lg}\frac{(\alpha^2-\theta^2)}{2} = W^{(w)}(\ell_w) \tag{10}$$

and similarly for wedge drying replacing θ with $\pi - \theta$ and $W^{(w)}$ with $W^{(d)}$. From this it follows that walls that exhibit continuous wetting or drying transitions produce wedges that exhibit continuous wedge wetting or drying with the divergence of ℓ_w being determined by the leading-order decay of the binding potential. If the wetting transition is first order on the other hand the filling transition is first order if $W^{(w)}(\ell)$ has an activation barrier and continuous if one is absent. Therefore even for first-order wetting the filling transition is continuous if the wedge wetting or drying temperature is lower than the corresponding spinodal temperature T_s for the wetting or drying transition. Since the wedge wetting (drying) temperature is necessarily lower than the wetting (drying) temperature, it follows that the tricritical wedge wetting (drying) temperature is lower than that for wetting and can be lowered arbitrarily by increasing the lilt angle α. This gives rise to the filling surface phase diagrams for SR-SR and LR-LR systems in Fig. 5(a) and Fig. 5(b) where we have emphasized the narrowing of the region of partial wedge wetting (drying) and the lowering of the tricritical point compared to Fig. 1(a) and Fig. 1(b). For SR-SR systems effective Hamiltonian studies predict that the exponents for continuous filling take universal values $\beta_w = \nu_\perp = 1/4$ and $\nu_y = 3/4$ [33], which have been measured accurately in Ising model simulation studies [34]. For LR-LR systems on the other hand, these studies predict that $\beta_w = 1/2$, $\nu_\perp = 1/4$, and $\nu_y = 1$, for dispersion forces ($p = 3$) and $\beta_w = 1/3$, $\nu_\perp = 1/4$, and $\nu_y = 5/6$ for retarded dispersion forces ($p = 4$).

For systems with imbalanced wall-fluid and fluid-fluid forces we still expect to see critical point wedge wetting and critical-point wedge drying even in the regions of the surface diagram where nonwetting occurs, see Figs. 5(c) and 5(d). For LR-SR systems, the line of first-order wetting transitions occurring for $\epsilon > \epsilon^c$ also gives rise to a line of wedge wetting transitions in this region. The expression Eq. (10) only involves the tail of the binding potential and so we may use the partial binding potential $\tilde{W}_{\rm LS}^{(w)}(\ell)$, which indicates that the wedge wetting transition is first order due to the presence of an activation barrier as in Fig. 2(b). Indeed, microscopic DFT studies of this for fluids adsorbed in right angle corners, indicate that the wedge wetting transition is strongly first order except extremely close to the bulk critical temperature. In this region numerical results are consistent with the filling transition being continuous, or very weakly first order [35], something which we clarify below. However, we also expect that LR-SR systems shows critical-point wedge drying even in the nonwetting gap for $\epsilon < \epsilon^c$. In this region of the phase diagram we may use the binding potential $W_{\rm LS}^{(d)}(\ell)$ in the MF expression (10) (and with θ replaced with $\pi - \theta$). This indeed predicts that a line of continuous wedge drying transitions persists in the nonwetting gap and converges to $C_{\rm ord}^{\infty}$. This expression identifies that the critical exponent $\beta_w = 1/2$ for dispersion forces ($p = 3$) and $\beta_w = 1/3$ for $p = 4$. Similarly we anticipate that for SR-LR systems a line of first-order wedge drying occurs for $\epsilon < \epsilon^c$ while a line of continuous wedge wetting still appears in the nonwetting gap. Both these

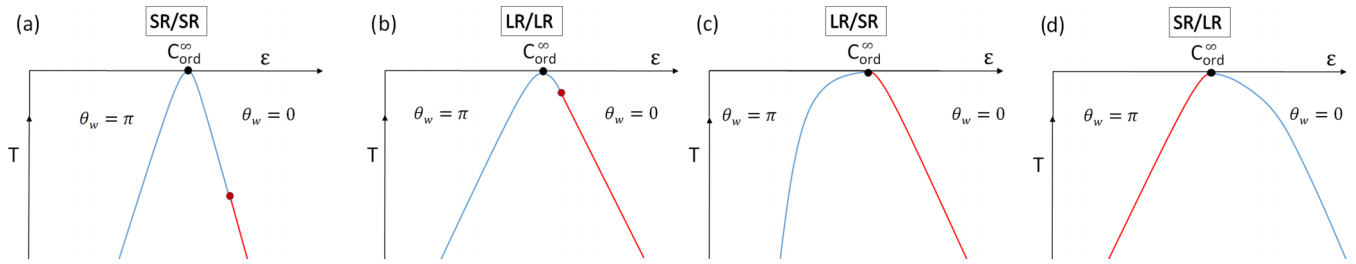

FIG. 5. Schematic surface diagrams for filling transitions (wedge wetting and wedge drying) for fluid adsorption in a wedge with opening angle $\pi - 2\alpha$, for the four possible scenarios SR-SR, LR-LR, LR-SR, and SR-LR for the ranges of the wall-fluid and fluid-forces. All systems exhibit critical-point filling, even in the presence of nonwetting, since the lines of wedge wetting and wedge drying converge to the location of the ordinary surface phase transition $C_{\rm ord}^{\infty}$. Lines of continuous (blue) and first-order (red) filling are shown as well as the regions of complete wedge wetting ($\theta_w = 0$) and drying ($\theta_w = \pi$) where the adsorbed liquid or gas layer film thickness $\ell_w = \infty$.

lines converge to $C^{\infty}_{\rm ord}$. The binding potential $W_{\rm SL}(\ell)$ for partial wetting in the nonwetting gap leads directly to a line of wedge wetting transition, occurring along $\theta = \alpha$, and identifies the exponent $\beta_w = 1/2$.

III. CRITICAL-POINT WEDGE DRYING WITHIN THE NONWETTING GAP

In this section we test the prediction that critical-point wedge filling occurs even within nonwetting gaps using a microscopic DFT to study fluid adsorption at a right angle corner. Our analysis extends an earlier study where we showed that, for LR-SR systems, a line of wedge wetting transitions occurs for the wedge-gas interface when the strength of the wall-fluid potential is large enough ($\epsilon > \epsilon^c$) [10,11]. Here we seek to show that within the nonwetting gap ($\epsilon < \epsilon^c$) a critical-point wedge drying transition occurs for the wall-liquid interface, prior to reaching T_c, and to determine the location and order of the transition. The presence of critical-point wedge drying in this region then shows that, for the planar wall-liquid interface, the limiting value of the contact angle at T_c is indeed $\theta = \pi$.

Within the framework of classical DFT the equilibrium density profile is found by minimizing the grand potential functional [36]

$$\Omega[\rho] = F[\rho] + \int d\mathbf{r}\rho(\mathbf{r})[V(\mathbf{r}) - \mu], \tag{11}$$

where $F[\rho]$ is the intrinsic Helmholtz free energy functional of the fluid one-body density, $\rho(\mathbf{r})$. Following a perturbative scheme modern DFT usually separates this as

$$F[\rho] = F_{\rm hs}[\rho] + \frac{1}{2}\iint d\mathbf{r}_1 d\mathbf{r}_2 \rho(\mathbf{r}_1)\rho(\mathbf{r}_2)\phi_{\rm att}(r_{12}), \tag{12}$$

where the first term on the right-hand side is the hard-sphere contribution. For this we use Rosenfeld's fundamental measure theory, which accurately models short-ranged repulsive correlations between the fluid atoms [37]. The final term in is a mean-field treatment of the attractive part, $\phi_{\rm att}(r)$, of the intermolecular fluid-fluid potential. Following our earlier study we take this to be a Lennard-Jones-like potential

$$\phi_{\rm att}(r) = -4\epsilon_{\rm ff}\left(\frac{\sigma}{r}\right)^6 H(r-\sigma), \tag{13}$$

which is truncated at $r_c = 2.5\,\sigma$, where σ is the hard-sphere diameter and $H(x)$ is the Heaviside function.

The external potential $V(\mathbf{r})$ arises from summing over all two-body wall-fluid interactions. That is $V(\mathbf{r}) \propto \int_{\mathcal{V}} d\mathbf{r}'\phi_{wf}(|\mathbf{r} - \mathbf{r}'|)$ where the integration is over the whole domain $\mathcal{V}$ of the wall, which is assumed to be a uniform distribution of atoms. Here $\phi_{wf}(r)$ is the wall-fluid two-body interaction, which for $r > \sigma$ we suppose decays algebraically modeling LR wall-fluid forces. We consider both $\phi_{\rm wf}(r) \propto r^{-6}$, modeling nonretarded dispersion forces, and $\phi_{\rm wf}(r) \propto r^{-7}$, for retarded dispersion forces. This will allow us to check the anticipated dependence of the critical exponents on the range of the wall-fluid interaction. The coefficients are chosen so that for a planar wall, the external potentials are given simply by

$$V_3(z) = -\frac{\epsilon_3}{z^3}, \qquad V_4(z) = -\frac{\epsilon_4}{z^4}, \tag{14}$$

for $z > \sigma$ (i.e., we have simply shifted the location of the hard wall to the $z = \sigma$ plane). The numerically determined surface phase diagrams for wetting and drying, together with the loci of lines of constant contact angle $\theta = \pi/4$ and $\theta = 3\pi/4$ are shown in Fig. 6, and are consistent with the qualitative structure expected for LR-SR systems [Fig. 1(c)]. Each exhibit a nonwetting gap between a line of first-order wetting transitions, occurring for $\epsilon > \epsilon^c_p$, and a line of temperature-independent drying transitions located exactly at $\epsilon = 0$. The only notable difference between these two surface phase diagrams, is that, as expected, the line of constant contact angle $\theta = 3\pi/4$, is more vertical, for $p = 3$ than $p = 4$. The lines of constant contact angle in these

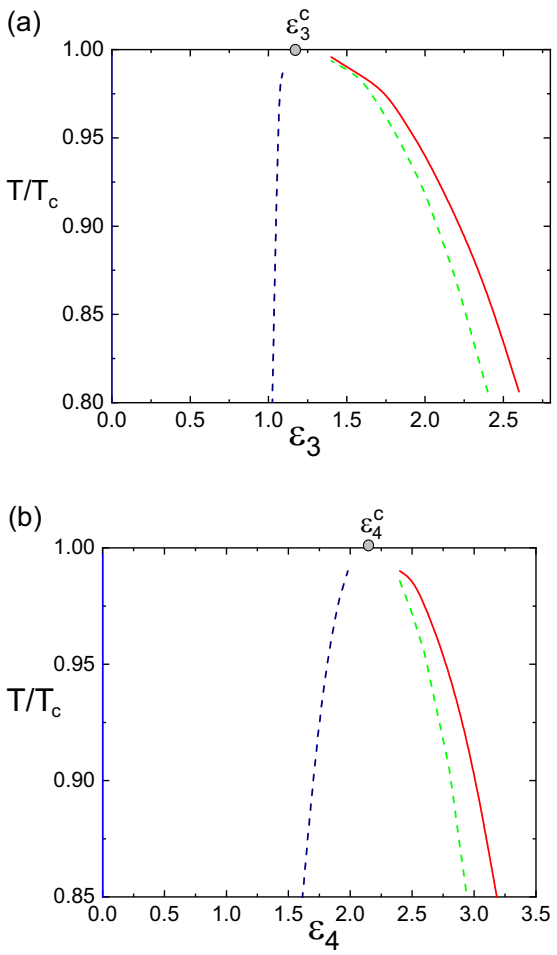

FIG. 6. DFT results for the wetting surface phase diagrams for LR-SR systems with external field decaying as $V(z) = -\epsilon_p/z^p$ for (a) $p = 2$ (dispersion forces) and b) $p = 3$ (retarded dispersion forces). The solid red lines correspond to first-order wetting transitions and the solid blue lines (located exactly at $\epsilon_p = 0$) are lines of continuous drying. A nonwetting gap appears between $\epsilon_p = 0$ and $\epsilon_p = \epsilon^c_p$, with $\theta \to \pi$ as $T \to T_c$ in this region. The loci of lines of constant contact angle $\theta = \pi/4$ and $\theta = 3\pi/4$ are shown as dashed green and dashed navy, respectively.

phase diagrams should determine the exact phase boundaries for wedge drying and wedge wetting at right angle corners ($\alpha = \pi/4$).

The corresponding external potentials $V_3(x, z)$ and $V_4(x, z)$ for right angle corners, defined in the Cartesian (x, z) plane, can also be determined analytically. For dispersion forces, the expression is quite simple and given by [35]

$$V_3(x, z) = -\frac{\epsilon_3}{2}\left[\frac{1}{z^3} + \frac{2z^4 + x^2z^2 + 2x^4}{2x^3z^3\sqrt{x^2+z^2}} + \frac{1}{x^3}\right]. \tag{15}$$

For retarded dispersion forces, it is a little more involved, and can be written [38]

$$V_4(x, z) = V_4(z) + \Delta V_4(x, z), \tag{16}$$

where

$$\Delta V_4(x, z) = -\frac{\epsilon_4}{6\pi}\frac{3\pi z^6 + 6xz^5 + 3\pi x^2z^4 + 4x^3z^3 + 6x^5z + 6(z^6 + z^4x^2 - x^4z^2 - x^6)\tan^{-1}\left(\frac{z}{x}\right)}{x^4(x^2+z^2)z^4}\Bigg], \tag{17}$$

outside of the hard-wall domain. It is straightforward to check to check that these expressions reduce to the corresponding planar ones (14), when x and z are far from the apex. While the present MF DFT treatment does not capture some of the fluctuation effects associated with continuous filling, notably the universal divergence of the roughness $\xi_\perp \propto (\theta - \alpha)^{-1/4}$, it should very accurately determine the location and order of the transition as well as the growth of the film thickness ℓ_w for systems with LR forces. We have determined the equilibrium free energies and density profiles at bulk coexistence from minimization of the functional $\Omega[\rho]$. This is done on an $L \times L$ grid (with $L = 50\sigma$ and $L = 100\sigma$ to check for finite-size effects) with discretization size $0.05\,\sigma$ using the same numerical scheme described in Ref. [39]. According to the thermodynamic predictions, the location of the wedge wetting and wedge drying temperatures T_{ww} and $T_{\rm wd}$, for given ϵ_p, follow from intersection with the curves of constant contact angle $\theta = \pi/4$ and $\theta = 3\pi/4$ respectively. To check this, we choose two values of ϵ_p either side of ϵ_p^c corresponding to wedge wetting and drying temperatures that are anticipated to be far from and close to T_c. Then, starting from different high-density and low-density configurations we numerical minimize $\Omega[\rho]$ looking for convergence to a unique density profile, indicative of continuous filling, and to two different profiles, indicative of first-order filling. The results are shown in Tables I and II, showing near perfect agreement between the observed and predicted locations of the filling phase boundary in all cases. The wedge drying transition is observed to be continuous at both high and low temperatures with the coverage of liquid at the apex, and corresponding film thickness ℓ_w, growing continuously as we approach the phase boundary, see Fig. 7. The measured value of the critical exponent β_w is in excellent agreement with the predictions $\beta_w = 1/3$ (for $p = 4$) and $\beta_w = 1/2$ (for $p = 3$), see Fig. 8. For the wedge wetting transitions on the other hand the transition is found to be strongly first order at low temperatures, since the value of ℓ_w is very small at the phase boundary, and weakly first order when T_{ww} is close to T_c where the film thickness ℓ_w is large. Figure 9 shows representative density profiles, for the wedge-gas interface, at these low- and high-temperature phase boundaries where the difference in the film thicknesses at coexistence is apparent.

IV. DISCUSSION

In this paper we have verified using a microscopic DFT model that critical-point wedge filling occurs even in the absence of critical-point wetting. More specifically, we have shown that for systems with LR wall-fluid and SR fluid-fluid forces, critical-point wedge drying occurs at a right angle corner even within the nonwetting gap part of the surface phase diagram, where there is no drying (or wetting) transition at any temperature. We find that the wedge wetting transition

TABLE I. Comparison between the thermodynamic predictions, $\theta(T_{ww}) = \pi/4$ and $\theta(T_{\rm wd}) = 3\pi/4$ for the locations of the wedge wetting and drying transitions for dispersion forces $p = 3$ at the right angle wedge and that obtained from DFT. The predicted orders of the transitions and the expected value of the critical exponent $\beta_w = 1/2$ are also verified. Here, $T^* = T/T_c$.

ε_3	1.10	1.15	1.50	2.10
Predicted $T^*_{\rm wd}$	0.980	0.993		
DFT $T^*_{\rm wd}$	0.984	0.997		
Predicted T^*_{ww}			0.989	0.900
DFT T^*_{ww}			0.991	0.905
Transition order	cont.	cont.	1st order	1st order
β_w	0.502	0.498		

TABLE II. Comparison between the thermodynamic predictions, $\theta(T_{ww}) = \pi/4$ and $\theta(T_{\rm wd}) = 3\pi/4$ for the locations of the wedge wetting and drying transitions for retarded dispersion forces $p = 4$ at the right angle wedge and that obtained from DFT. The predicted orders of the transitions and the expected value of the critical exponent $\beta_w = 1/3$ are also verified.

ε_4	1.75	2.00	2.50	2.75
Predicted $T^*_{\rm wd}$	0.922	0.994		
DFT $T^*_{\rm wd}$	0.927	0.992		
Predicted T^*_{ww}			0.972	0.920
DFT T^*_{ww}			0.970	0.916
Transition order	cont.	cont.	1st order	1st order
β_w	0.335	0.329		

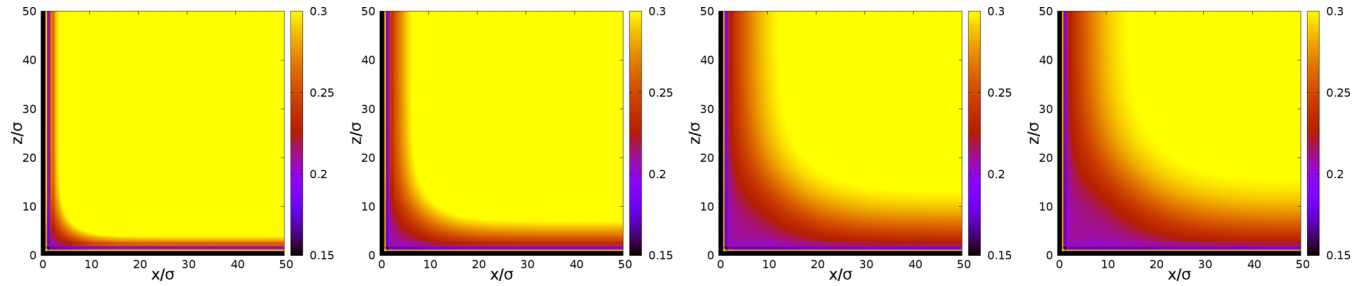

FIG. 7. DFT results showing the continuous growth of an adsorbed gas layer, at a wedge-liquid interface, on approaching a continuous wedge drying transition at $T^*_{\rm wd} \approx 0.995\,T_c$ with retarded dispersion forces ($p = 4$).

is first order, albeit weakly, when T_{ww} is close to T_c, while the wedge drying transition is continuous with the growth of the filling layer thickness in excellent agreement with the expected values of the critical exponent $\beta_w = 1/3$ (for retarded dispersion forces) and $\beta_w = 1/2$ (for dispersion forces).

The argument we have proposed for the necessity of critical-point filling in all systems is very different from the original (and flawed) Cahn argument for the necessity of

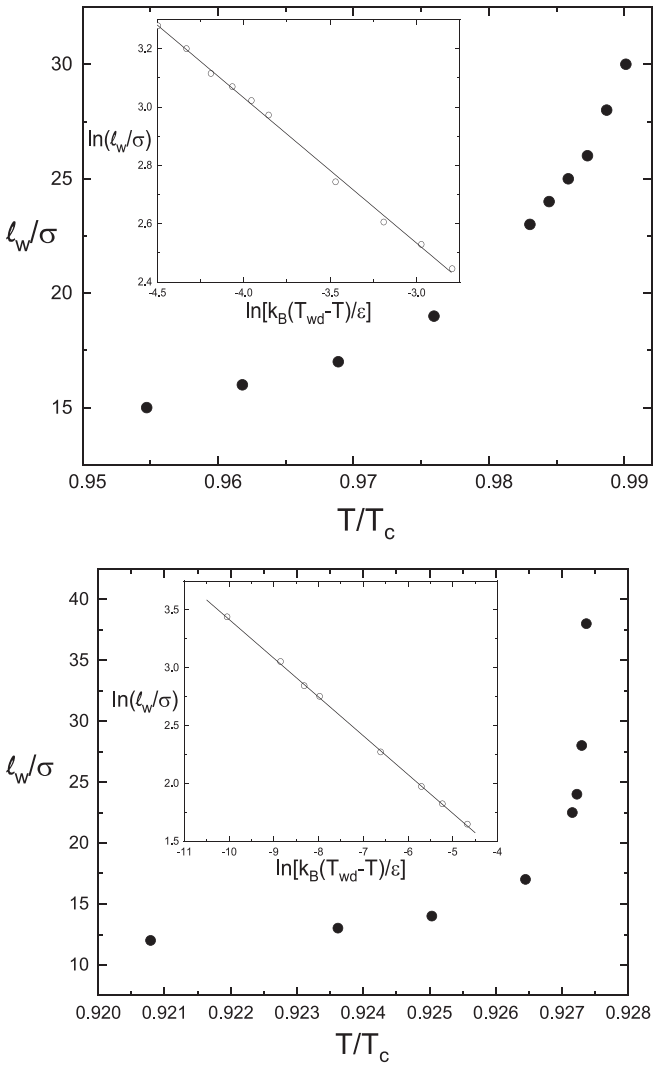

FIG. 8. DFT results showing the growth of the thickness ℓ_w of the gas layer at the right-angle wedge on approaching the drying transitions for dispersion forces ($p = 3$, $\epsilon_w = 1.15$) (top panel) and retarded forces ($p = 4$, $\epsilon_w = 1.75$) (bottom panel). Insets show the excellent agreement with the predictions $\beta_w = 1/2$ (for $p = 3$) and $\beta_w = 1/3$ (for $p = 4$) with the fitted exponents shown in Table 1.

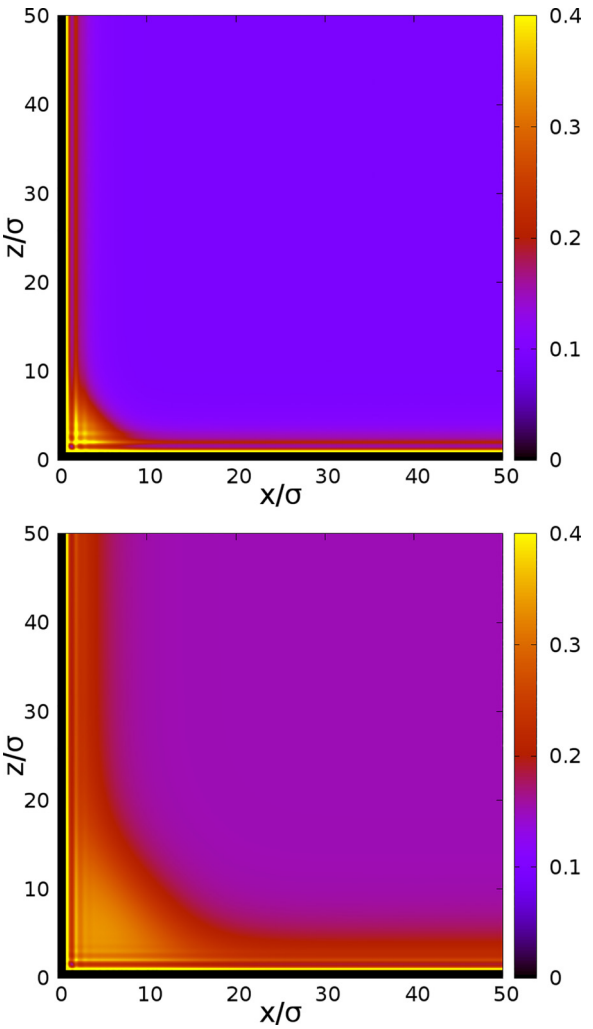

FIG. 9. DFT results for retarded dispersion forces showing the density profiles of the wedge-gas interface at the wedge wetting phase boundary, $\theta = \pi/4$, at a low temperature ($T_{ww} = 0.915\,T_c$), where the transition is strongly first order (top panel), and at a high temperature ($T_{ww} = 0.973\,T_c$), where it is weakly first order (bottom panel).

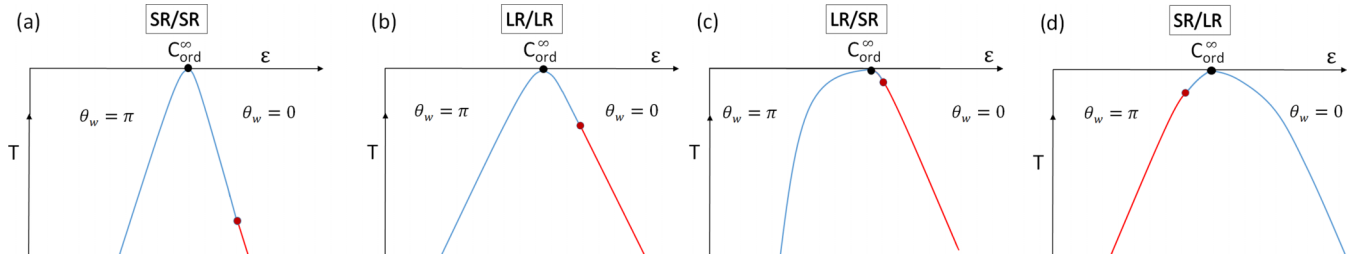

FIG. 10. Schematic surface diagrams for filling transitions for fluid adsorption in a cone geometry (with tilt angle α, as in Fig. 4) for the four possible scenarios for the ranges of the wall-fluid and fluid-fluid forces. All systems exhibit critical-point filling with SR-SR,LR-LR and LR-SR systems all showing continuous conic drying and both first-order and continuous conic wetting, with the location of the tricritical point increasingly close to T_c in (a)–(c). The order of the conic filling transitions is reversed for SR-LR systems.

critical-point wetting. The Cahn argument relied on a hypothesis for the decrease in the relative values of the wall-gas and wall-liquid surface tensions, compared to the liquid-gas tension, as $T \to T_c$, which certainly does not hold when there is an imbalance of the ranges of wall-fluid and fluid-fluid forces. The necessity of critical-point wedge filling on the other hand follows from the general requirement that, at least for simple fluids, the loci of lines of constant contact angle $\pi > \theta > 0$ must, in general converge to an ordinary surface phase transition at T_c. This is entirely in keeping with the scaling theory proposed by Nakanishi and Fisher for wetting in systems with SR forces but actually applies much more generally, even in the presence of LR wall-fluid and/or fluid-fluid forces. This is the reason the wedge filling phase diagrams, shown schematically in Fig. 5, for different combinations of the wall-fluid and fluid-fluid forces, are very similar to each other, compared to the different types of surface phase diagram for wetting (Fig. 1).

Finally, we mention that the necessity of critical-point filling also applies to fluids adsorbed in conic geometries since the thermodynamic conditions for wedge wetting (6) and wedge drying (7) remain the same. In this case we anticipate that the order of the filling transition is determined by the sign of the line tension τ with a positive or negative τ leading to first-order or continuous cone filling [40]. Within the effective Hamiltonian theory developed by Indekeu and coworkers, a positive line tension only arises if the activation barrier $W(\ell)$ is sufficiently large, i.e., if the wetting transition is sufficiently strongly first order [41]. This implies that the surface phase diagrams for filling in a cone are qualitatively the same, see Fig. 10. SR-SR, LR-LR, and LR-SR systems each show a line of continuous conic drying while conic wetting is first order at low temperatures and continuous closer to T_c. For SR-LR systems this is reversed and the line of conic drying breaks into first-order and continuous sections with conic wetting always being continuous. The critical singularities characterizing conic filling are universal, independent of the range of the intermolecular forces, and similar to wedge covariance in two dimensions, bear a striking similarity to the renormalization group predictions for the strongest possible fluctuation regime of three-dimensional short-ranged critical wetting [40]. For SR-SR and LR-SR systems these predictions can be tested in microscopic DFT similar to the study reported here and also in simulations.

To close, we return to the conditions regarding critical-point wetting and nonwetting in other systems, which may have analogues of wedge filling. While this does not seem feasible in fluid mixtures, wetting and nonwetting also occur along grain boundaries, for example, near defect lines in simple Ising systems. Unlike a wall, a defect line does not induce a surface coupling analogous to a surface field (unless the bulk couplings either side of the boundary are modified) and does not have the impenetrable hard-wall constraint. Studies of these systems show that nonwetting may persist up to T_c even for systems with SR forces and that the limiting value of the contact angle is $\pi/2$ [42,43]. By deforming the defect line into a corner, or indeed a kink, of arbitrary angle, however, we may induce an analogous grain boundary filling transition, prior to T_c even in the presence of nonwetting, which may be studied in simple Landau square gradient theory.

ACKNOWLEDGMENTS

We thank Dr. C. Rascón for many helpful discussions. A.M. acknowledges the support of the grant supported by the Czech Science Foundation, Project No. 21-27338S.

[1] J. W. Cahn, J. Chem. Phys. **66**, 3667 (1977).
[2] C. Ebner and W. F. Saam, Phys. Rev. Lett. **38**, 1486 (1977).
[3] D. E. Sullivan and M. M. Telo da Gama, in *Fluid Interfacial Phenomena*, edited by C. A. Croxton (Wiley, New York, 1985).
[4] S. Dietrich, in *Phase Transitions and Critical Phenomena*, edited by C. Domb and J. L. Lebowitz (Academic, New York, 1988), Vol. 12.
[5] M. Schick, in *Liquids and Interfaces*, edited by J. Chorvolin, J. F. Joanny, and J. Zinn-Justin (Elsevier, New York, 1990).
[6] G. Forgacs, R. Lipowsky, and Th. M. Nieuwenhuizen, in *Phase Transitions and Critical Phenomena*, edited by C. Domb and J. L. Lebowitz (Academic, London, 1991), Vol 14.
[7] D. Bonn, J. Eggers, J. Indekeu, J. Meunier, and E. Rolley, Rev. Mod. Phys. **81**, 739 (2009).
[8] M. P. Nightingale and J. O. Indekeu, Phys. Rev. B **32**, 3364 (1985).
[9] R. Evans, M. C. Stewart, and N. B. Wilding, Proc. Natl. Acad. Sci. USA **116**, 23901 (2019).

[10] A. O. Parry and A. Malijevský, Phys. Rev. Lett. **131**, 136201 (2023).
[11] A. O. Parry, C. Rascón, and A. Malijevský, J. Phys. Condens. Matter **36**, 17LT01 (2024).
[12] H. Nakanishi and M. E. Fisher, Phys. Rev. Lett. **49**, 1565 (1982).
[13] C. Ebner and W. F. Saam, Phys. Rev. B **35**, 1822 (1987).
[14] J. S. Rowlinson and B. Widom, *Molecular Theory of Capillarity* (Clarendon, Oxford, 1989).
[15] P. G. de Gennes, C. R. Acad. Sci. Paris **297**, 9 (1983).
[16] V. Privman, J. Chem. Phys. **81**, 2463 (1984).
[17] J. O. Indekeu and K. Koga, Phys. Rev. Lett. **129**, 224501 (2022).
[18] E. Brézin, B. I. Halperin, and S. Leibler, Phys. Rev. Lett. **50**, 1387 (1983).
[19] M. E. Fisher and A. J. Jin, Phys. Rev. B **44**, 1430 (1991).
[20] R. Evans, D. C. Hoyle, and A. O. Parry, Phys. Rev. A **45**, 3823 (1992).
[21] J. R. Henderson, Phys. Rev. E **50**, 4836 (1994).
[22] A. O. Parry, J. M. Romero-Enrique, and A. Lazarides, Phys. Rev. Lett. **93**, 086104 (2004).
[23] A. O. Parry, C. Rascón, N. R. Bernardino, and J. M. Romero-Enrique, Phys. Rev. Lett. **100**, 136105 (2008).
[24] A. Squarcini, J. M. Romero-Enrique, and A. O. Parry, Phys. Rev. Lett. **128**, 195701 (2022).
[25] S. Dietrich and M. Napiórkowski, Phys. Rev. A **43**, 1861 (1991).
[26] A. O. Parry and C. Rascón, Soft Matter **19**, 5668 (2023).
[27] R. Finn, Equilibrium capillary surfaces, in *Grundlehren der Mathematischen Wissenschaften* (Springer, New York, 1986), Vol. 284.
[28] P. Concus and R. Finn, Proc. Natl. Acad. Sci. USA **63**, 292 (1969).
[29] E. H. Hauge, Phys. Rev. A **46**, 4994 (1992).
[30] A. O. Parry, C. Rascón, and A. J. Wood, Phys. Rev. Lett. **83**, 5535 (1999).
[31] A. O. Parry, M. J. Greenall, and A. J. Wood, J. Phys.: Condens. Matter **14**, 1169 (2002).
[32] G. Delfino and A. Squarcini, Phys. Rev. Lett. **113**, 066101 (2014).
[33] A. O. Parry, C. Rascón, and A. J. Wood, Phys. Rev. Lett. **85**, 345 (2000).
[34] A. Milchev, M. Müller, K. Binder, and D. P. Landau, Phys. Rev. Lett. **90**, 136101 (2003).
[35] A. Malijevský and A. O. Parry, Phys. Rev. Lett. **110**, 166101 (2013).
[36] R. Evans, Adv. Phys. **28**, 143 (1979).
[37] Y. Rosenfeld, Phys. Rev. Lett. **63**, 980 (1989).
[38] A. Malijevský and A. O. Parry, Phys. Rev. E **93**, 040801(R) (2016).
[39] A. Malijevský and A. O. Parry, J. Phys.: Condens. Matter **25**, 305005 (2013).
[40] A. O. Parry, A. J. Wood, and C. Rascón, J. Phys.: Condens. Matter **13**, 4591 (2001).
[41] J. O. Indekeu, Int. J. Mod. Phys. B **08**, 309 (1994).
[42] A. Sevrin and J. O. Indekeu, Phys. Rev. B **39**, 4516 (1989).
[43] F. Igloi and J. O. Indekeu, Phys. Rev. B **41**, 6836 (1990).